Physical justification for the time resolution limit of silicon planar detectors of long-range heavy ions

© V.K. Eremin, N.N. Fadeeva, E.M. Verbitskaya¶, I.V. Eremin

Ioffe Institute,
194021 St. Petersburg, Russia
¶ E-mail: elena.verbitskaya@ioffe.mail.ru

Received May 6, 2024
Revised August 16, 2024
Accepted August 26, 2024

A model of current outflow from the track plasma of a long-range heavy ion irradiating a silicon p^+-n-n^+-detector is presented. Basing on the model, an analytical description of the process was obtained and its numerical simulation was performed. The results on the coordinate and temporal transformation of the electric field and carrier concentrations N_{pl} in plasma and the current signal shape show good quantitative agreement between the calculation and simulation data. The rise time of the current signal is not limited by the carrier outflow from the plasma and is controlled by the track creation time in few ps, which determines the physical limit of the detector time resolution when registering long-range ions. The signal decay contains two components, a fast polarization component associated with the formation of layers with high electric field near the p^+- and n^+-contacts, whose duration reduces from 480 to 100 ps as N_{pl} rises from $1 \cdot 10^{15}$ to $1 \cdot 10^{17}$ cm^{-3}, and a slow relaxation component, caused by the depletion of the electron-hole plasma in track.

Keywords: silicon detector, long-range ions, polarization, time resolution.

DOI: 10.61011/SC.2024.06.59455.6643

1. Introduction

Silicon charged-particle detectors are used widely in high-energy and nuclear physics. Compactness, simplicity of design, and manufacturability set the trends in their development and specify their field of application. One steady trend in experimental nuclear physics is the growth of intensity of ion beams and expansion of the range of ion masses and energies. Separators of nuclear fragments (high-energy ions) have become a necessary element of accelerator complexes: they allow one to track the passage of an individual particle through the beam-shaping system and monitor a complete set of its parameters (charge, energy, mass, and time of entry into the nuclear experiment region). In this context, accelerator technology and physical experiments require instruments for *in-flight* determination of the characteristics of individual ions based on their trajectories in the magnetic beam control system with the use of arrays of position-sensitive detectors and simultaneous high-precision measurement of their velocity by the time-of-flight (ToF) method.

Silicon detectors of high-energy ions and particles are an established class of devices that are suitable for spectrometry with a high energy resolution. A short-range ion stops in the sensitive region of a detector, forming a track of electron–hole ($e-h$) pairs with length r_i that is smaller than detector thickness d. The value of r_i depends on the mass and energy of the ion, and the number of non-equilibrium charge carriers (NECCs) is proportional to the energy. The analysis of shape of the electrical response of a detector revealed that the signal rise delay time exceeds the expected one derived from the carrier drift time in the sensitive region [1–4]. This has a negative effect on the time and energy resolution and was called the plasma delay, which is related to the formation of plasma with high concentration N_{pl} of $e-h$ pairs in an ion track. Plasma lifetime t_{pl} was < 10 ns and depended on electric field strength E in the detector and the ion mass, limiting the accuracy of time measurements to several hundred picoseconds. Quantitative models of current outflow from plasma included the processes of extraction of electrons and holes from the end of a track under the influence of an electric field by the space-charge-limited current (SCLC) mechanism, their subsequent drift, and diffusion outflow of carriers from the side track surface [1].

The above-mentioned *in-flight* ion separation with silicon detectors [5–8] is planned to be implemented at the Super Fragment Separator at the GSI Helmholtz Centre for Heavy Ion Research (Darmstadt, Germany). The problem has become especially relevant in the context of studies of „exotic" high-energy ions with range r_i in silicon that exceeds d significantly [9–12]. Exotic ions have anomalous proton-to-neutron ratios, are produced in random interactions of heavy nuclei with a heavy thin-film target, and have unpredictable characteristics. Therefore, any experiments in this field require the ion mass to be determined with an accuracy of ~ 1 a.m.u. This may be achieved with a time resolution of detectors no worse than 30 ps if, e. g., a uranium ion with an energy of several hundred GeV needs to be characterized and the ToF spectrometer flight base length is ~ 50 m. The feasibility of such a resolution for silicon planar detectors with a p^+-n junction was demonstrated at GSI, where signals from ^{197}Au and ^{132}Xe isotopes with energies of hundreds of GeV were recorded by a digital oscilloscope

with an analog bandwidth of 2 GHz. Although a significant plasma delay was expected, the rise time (front) of the current signal turned out to be significantly shorter than 1 ns, and the time resolution estimated by the variance of front fluctuations was better than 30 ps [6–8]. A qualitative model of current outflow from plasma of a long-range heavy ion track was developed in order to explain the obtained result. According to this model, the rise time of the current response of a semiconductor detector is specified by the kinetics of plasma polarization in the track and may assume a value of several tens of picoseconds [6].

In addition to fundamental implications, this research has an important applied aspect in the analysis of influence of heavy ions on electronic components (the so-called single event effect), which is carried out at the Super Proton Synchrotron accelerator complex at CERN [13]. In Russia, similar experiments are planned to be carried out at the Nuclotron-based Ion Collider fAcility (NICA) that is being constructed at the Joint Institute for Nuclear Research in Dubna and should provide the means for testing of encapsulated microchips and space radiobiological research (ion energies of 150–500 and 400–1100 MeV/nucleon, respectively) [14].

In the present study, we continue the research on kinetics of the current response of silicon p^+-n-n^+-detectors in the case of ion penetration throughout the entire sensitive volume. The aim of this study is to establish a physical justification for the shape of a signal with a short rise time and acquire new data differing from those reported earlier in [6,15]. Analytical calculations and numerical modeling of the processes of electron and hole outflow from an ion track at different values of N_{pl} were performed. Data on the coordinate and temporal transformation of profiles of the electric field strength and NECC concentrations and the formation of a current pulse were obtained. In order to analyze the processes occurring at the initial stage of current outflow from a track and shaping the detector signal front, calculations were carried out in the 1D geometry, which made it possible to identify characteristic stages of the process, characterize them analytically, and obtain quantitative estimates.

2. 1D model of a long-range ion track in a silicon detector

Figure 1, where x is the coordinate normal to the detector surface, illustrates the discussed 1D model of kinetics of electrons and holes outflow from a track formed in a silicon detector by a long-range ion with range $r_i > d$. Within the detector, the track is a cylinder filled uniformly with $e-h$ pairs. Their concentration N_{pl} in the cross section is the primary physical parameter governing the outflow of carriers from the track.

The aim of the present study is to establish the time resolution limit of silicon detectors in the process of detection of long-range heavy ions. Therefore, it is important to choose

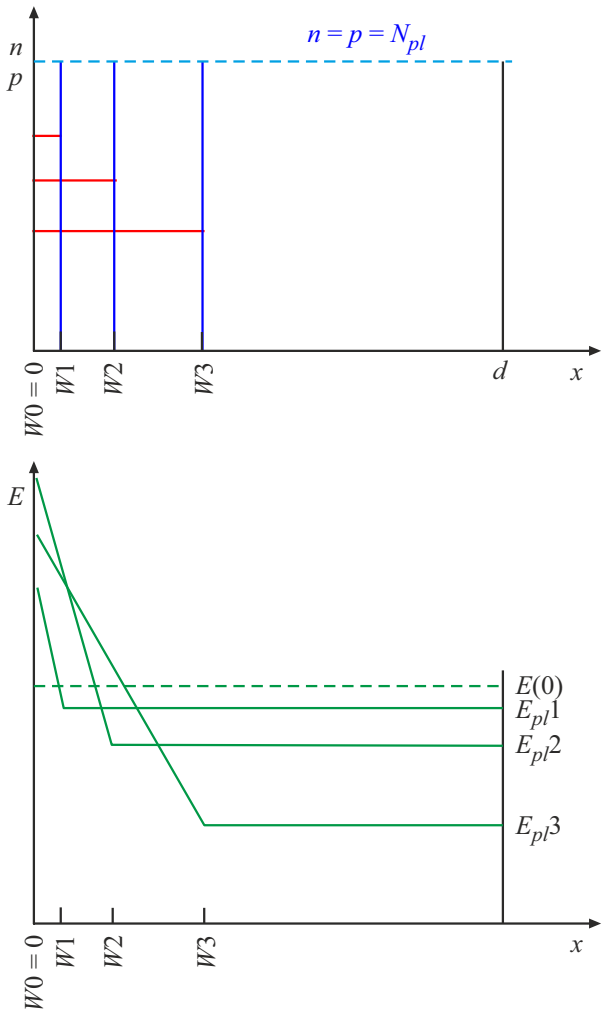

Figure 1. Model of temporal transformation of distributions of electrons $n(x)$ and holes $p(x)$ (blue and red lines, respectively) and electric field strength $E(x)$ in the sensitive region of the detector interacting with a long-range heavy ion. W is the thickness of the track polarization layer near the p^+-contact.

a proper time interval within which calculations and simulations are performed. Since a subnanosecond resolution is needed to optimize ToF diagnostics, processes evolving on the scale of units of nanoseconds were examined with a picosecond level of detail.

It should be emphasized that processes within the track of a single isolated ion are considered. Therefore, the issues of local homogeneity of the concentration of $e-h$ pairs along the track and the kinetics of charge losses due to NECC trapping by defects, which emerged in the course of its formation, are subject to analysis.

1) Fluctuations of the number of $e-h$ pairs in particle tracks have been studied extensively in the context of their influence on the ultimate resolution of semiconductor detectors. It was demonstrated that the standard deviation of the number of pairs in a particle track is given by $\sqrt{FN}$, where N is the number of formed pairs and F is the Fano

factor. It is assumed in the discussed model of current outflow from a track that this track is a cylinder with a diameter of $1\,\mu$m (cross-section area $S = 0.8 \cdot 10^{-8}\,\text{cm}^2$). The characteristic length within which fluctuations of the number of pairs may be significant for current outflow modeling is determined with the temporal accuracy of characterization of processes in the track relevant to ToF diagnostics (i.e., $\sim 10^{-11}$ s) and depends on drift velocity v of outflowing NECCs. Setting v to 10^7 cm/s (i.e., close to saturation velocity v_s), we find characteristic length 10^{-4} cm within which an average of 800 $e{-}h$ pairs form at $N_{pl} = 10^{15}\,\text{cm}^{-3}$. The expected fluctuation of their number at $F = 0.12$ is $\sqrt{FN} \approx 10$ (i.e., $\sim 1\%$), which is insignificant for the considered model.

2) The process of interaction of ions with atoms of the silicon crystal lattice was simulated in SRIM (Stopping and Range of Ions in Matter) to assess the influence of formation of radiation-induced defects on the carrier lifetime. Long-range ^{238}U ions with an energy of 40 GeV ($r_i = 3.6$ mm) were used as an example. The corresponding number of primary vacancies formed within a track $300\,\mu$m in length was 8240 per ion. Since only 2% of vacancies are involved in the formation of electrically active defect complexes, the number of carrier trapping centers within the track of a single ^{238}U ion does not exceed ~ 160, which corresponds to their concentration $N_{tr} = 6.7 \cdot 10^{11}\,\text{cm}^{-3}$ at a track volume of $2.4 \cdot 10^{-10}\,\text{cm}^3$. Therefore, carrier trapping time constant $\tau_{tr} = (\sigma v_{th} N_{tr})^{-1}$ assumes a value of $0.15 \cdot 10^{-3}$ s at typical trapping cross section $\sigma = 10^{-15}\,\text{cm}^2$ and thermal carrier velocity $v_{th} = 10^7$ cm/s at room temperature. Since this parameter is the one that governs the recombination of non-equilibrium carriers in semiconductors with an indirect band gap (silicon included [16]) and its value is significantly greater than the time interval considered in the kinetics of carrier outflow from the track, the processes of NECC trapping and recombination of $e{-}h$ pairs in the track of a heavy ion do not affect the carrier concentration in track plasma and the kinetics of the current response of a detector. In view of this fact and the weakness of ionization fluctuations, N_{pl} is assumed to remain constant in the process of carrier outflow from the track.

3) The temporal transformation of a track due to diffusion in the radial direction was not considered, since the change in carrier concentration on the track axis within $t = 10$ ps does not exceed 5%.

It was also taken into account that track plasma and the surrounding volume of the sensitive region of the detector are electrically neutral, which is why the radial component of the electric field is lacking not only at the onset of carrier outflow from plasma, but also at the later stages of this process, justifying the use of the 1D model.

With the considerations listed in paragraphs 1 and 2 in mind, we presented the distributions of electron and hole concentrations at the p^+-contact within the model of temporal transformation of the ion track in a detector based on high-resistance silicon at four points in time: moment $t_0 = 0$ of track formation and subsequent moments t_1, t_2, and t_3 (Figure 1). At $t = t_0$, the track is bounded by contacts at $x = 0$ and $x = d$, and the corresponding electric field $E(0) = V/d$ (where V is the applied voltage) is uniform.

Since $e{-}h$ pairs within the track are affected by electric field $E(0)$, electrons and holes start to drift toward the corresponding contacts. In this case, electrons drift with a velocity of $\mu_n E$ (where μ is the carrier mobility) toward the positively charged n^+-contact as a packet with boundary W (solid blue lines), while holes outside of plasma drift toward the p^+-contact, which is under a negative potential. Therefore, the positive charge of drifting holes with concentration p_p in the $[0{-}W]$ layer will enhance the electric field strength near the p^+-contact (Figure 1) in accordance with the Poisson equation:

$$\frac{dE}{dx} = \frac{ep_p}{\varepsilon\varepsilon_0}, \tag{1}$$

where e is the elementary charge and ε and ε_0 are the permittivities of silicon and vacuum, respectively, at boundary condition $E(W) = E_{pl}$, where E_{pl} is the electric field strength in the track plasma region.

Assuming that the increase in E in the polarization layer formed near the p^+-contact is significant and leads to saturation of the drift velocity of holes to v_{ps}, the condition of continuity of current in the structure is written as

$$ep_p v_{ps} W = eN_{pl}\mu_n E_{pl}, \tag{2}$$

where the left-hand side defines the current of holes drifting with velocity v_{ps} in layer W and the right-hand side characterizes the corresponding velocity of electron packet motion to the n^+-contact in the track plasma region. It is evident that expression (2) establishes a connection between thickness W of the polarization layer and field strength E_{pl} in the region of electrically neutral plasma. According to Eq. (1), average field strength $\langle E_p \rangle$ in the polarization layer is determined in this case as

$$\langle E_p \rangle = E_{pl} + \frac{ep_p W}{\varepsilon\varepsilon_0} \tag{3}$$

at maximum $E_{\max\_p}$ at the p^+-contact equal to

$$E_{\max\_p} = E_{pl} + 2\,\frac{ep_p W}{\varepsilon\varepsilon_0}. \tag{4}$$

The last condition shaping the current response of a detector is the constancy of voltage V applied to it:

$$V = E_{pl}(d - W) + \langle E_p \rangle W, \tag{5}$$

which follows from the field structure shown in Figure 1. Inserting expressions (2) and (3) into (5), we obtain a relation between E_{pl} and W, which is determined by the drift parameters of electrons and holes:

$$E_{pl} = \frac{V}{d - W}\left[1 + \frac{W}{d - W} + \frac{eN_{pl}\mu_n W^2}{2v_{sp}\varepsilon\varepsilon_0(d - W)}\right]^{-1}. \tag{6}$$

Thus, analysis of the proposed model of current outflow from plasma of a long-range heavy ion track revealed the existence of a direct relation between the electric field strength in the $e-h$ plasma region and width W of the polarization layer (Eq. (6)). The kinetics of variation of E_{pl} and the other characteristics in the process of current outflow was determined as a transition from $E_{pl}(W)$ to $E_{pl}(t)$ in accordance with Eq. (7) that was performed numerically based on relation

$$\frac{dW(t)}{dt} = \mu E_{pl}(t), \tag{7}$$

which yields the kinetics of density $J(t)$ of the detector current response expressed, according to Eq. (2), as

$$J(t) = eN_{pl}\mu_n E_{pl}(t). \tag{8}$$

The considered mechanism of outflow of hole and electron current from ion plasma at the negatively charged p^+-contact is an illustration of physical processes of formation of the current response of a detector to the incidence of a heavy ion. In an actual $p-i-n$ structure, a similar mechanism of current outflow and electric field transformation also operates at the n^+-contact. The only difference is that a hole packet shifts under the influence of an electric field in plasma and outflowing electrons drift in the field of the polarization layer to the n^+-contact. It is evident that the base conditions of continuity of current flowing in the structure and constancy of the applied voltage must be preserved, and this specifies quantitatively the kinetics of variation of the electric field strength and the current response shape. The qualitative patterns in signal formation also remain unchanged.

The 1D model of a long-range ion track presented above was used in analytical calculation of the kinetics of processes within the track near the p^+-contact. Calculations were performed on a grid of determined parameters (with the initial one being the value of W_p that was set with a pitch of $0.2\,\mu$m).

The kinetics of variation of the electric field strength profiles across the detector thickness and the outflow of electrons and holes generated in the track were also simulated within the 1D model of a long-range ion track. This simulation was performed with the use of proprietary software that incorporated a fundamental system of equations characterizing the continuity of current, the formation of an electric field, and the diffusion-drift carrier transport. Diffusion in the x direction and the dependence of drift velocity on the electric field strength were taken into account. Time t_0 elapsed from the moment of ion entry into the detector was the initial parameter for simulation. Detailed distributions of the electric field strength and electron and hole concentrations on a coordinate grid with a pitch of $x = 0.005\,\mu$m were obtained.

Calculations and modeling were performed for a p^+-n-n^+-detector based on n-Si with a resistivity of $2\,\text{k}\Omega\cdot\text{cm}$ (effective charge concentration $N_{\text{eff}} = 1.7\cdot 10^{12}\,\text{cm}^{-3}$ in the sensitive region), $d = 300\,\mu$m, and thin p^+- and n^+-contact layers doped with boron and phosphorus to a concentration of $\geq 1\cdot 10^{18}\,\text{cm}^{-3}$. An aluminum film, which was neglected in analytical calculations, was deposited onto the surface of p^+- and n^+-layers. The modeled contact structure was a combination of a heavily doped layer and an aluminum film; the doping profiles of p^+- and n^+-layers were also taken into account. The applied voltage was 200 V in both analytical calculations and modeling. This voltage provided a virtually uniform $E(0)$ profile with a strength of $\sim 6.7\cdot 10^3$ V/cm.

Calculations and modeling were performed for three values of N_{pl} characteristic of ions with energies of several hundred GeV and masses ranging from 50 a.m.u. to the mass of uranium isotopes: $1\cdot 10^{15}$, $1\cdot 10^{16}$, and $1\cdot 10^{17}\,\text{cm}^{-3}$.

3. Results of simulation and calculation of plasma dissipation kinetics in a track of a long-range ion

Figure 2 shows the simulated electric field strength profiles within the time interval of 1 ps–4 ns (axis Y is logarithmic in scale) under the influence of ions with concentration $N_{pl} = 1\cdot 10^{15}\,\text{cm}^{-3}$.

Electric field strength $E(x)$ decreases linearly from the p^+-contact to the n^+- one in accordance with the concentration of charged donors in the n region at $t = 0$. Its gradient decreases over time due to the redistribution of carriers in the plasma volume until the sensitive volume becomes completely electrically neutral ($N_{\text{eff}} = dE/dx = 0$). This process is characterized by Maxwell relaxation time $t_M = \varepsilon\varepsilon_0/e\mu N_{pl}$, which is ~ 6 ps for $N_{pl} = 1\cdot 10^{15}\,\text{cm}^{-3}$.

The process of significant transformation of the electric field strength profiles near the contacts is initiated alongside

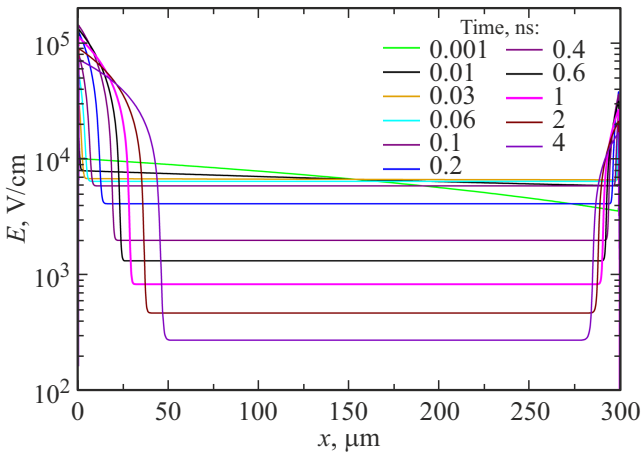

Figure 2. Temporal evolution of simulated electric field strength profiles in a silicon p^+-n-n^+-detector irradiated with ions. $N_{pl} = 1\cdot 10^{15}\,\text{cm}^{-3}$. (A color version of the figure is provided in the online version of the paper).

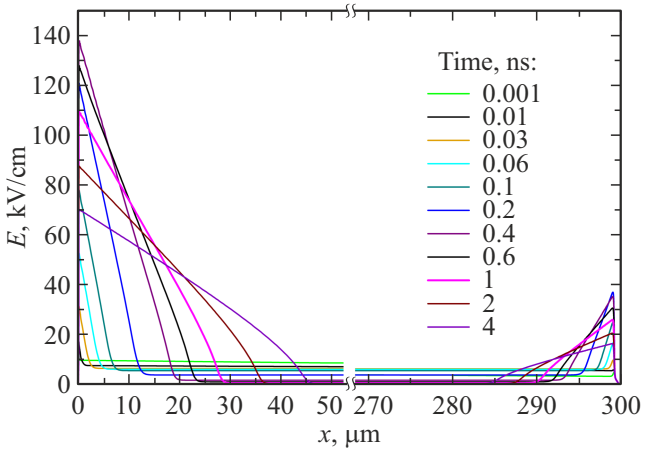

Figure 3. Fragments of the electric field strength profiles near the p^+- and n^+-detector contacts at different points in time. $N_{pl} = 1 \cdot 10^{15}\,\mathrm{cm}^{-3}$.

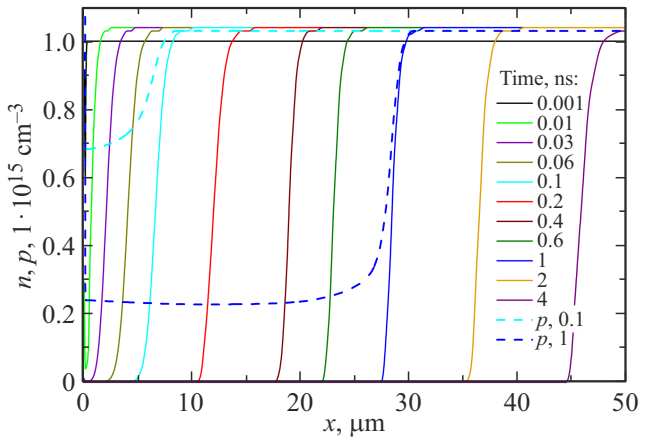

Figure 4. Distributions of electron and hole concentrations (solid and dashed curves, respectively) near the p^+-contact of a silicon detector at different t. $N_{pl} = 1 \cdot 10^{15}\,\mathrm{cm}^{-3}$.

with the restoration of electrical neutrality of plasma (Figure 3). Regions with strength maxima $E_{\max}$ emerge directly at the contacts, which is attributable to track polarization. In the extended middle region, the electric field strength remains constant at E_{pl}; notably, both E_{pl} and the width of these regions decrease with time. Inequality $E_{\max\_p} > E_{\max\_n}$ is fulfilled at all concentrations of $e-h$ pairs within the track, and at $N_{pl} = 1 \cdot 10^{15}\,\mathrm{cm}^{-3}$ $E_{\max\_p}$ exceeds the field strength in the middle region by several orders of magnitude.

The temporal variation of electron concentration near the p^+-contact is presented in Figure 4 for $N_{pl} = 1 \cdot 10^{15}\,\mathrm{cm}^{-3}$. It can be seen that concentration $n(x)$ in the layer near the p^+-contact approaches zero within 20–30 ps as a result of drift of electrons to the n^+-contact in the form of a packet retaining a sharp boundary at $x = W_p$. The electron concentration in the drifting packet itself does not vary with coordinate and is close to N_{pl}. In the W_p region where electrons are virtually lacking, holes drift toward the p^+-contact, thus forming a peak of the field strength. Two curves for concentration $p(x)$ are shown for comparison in Figure 4. At $t = 1$ ns, this concentration is 7 orders of magnitude higher than n and, consequently, governs the field strength distribution in the polarization layer. At later points in time, p also decreases due to hole drift to the p^+-contact, but remains significant compared to $n(x)$.

The $E(x)$ profiles in polarization layers exhibit constant gradients only at the initial stage of current outflow from plasma (Figure 3). The absolute N_{eff} values at contacts decrease at later times t, preserving their sign and inducing an increase in W. It is characteristic that the electric field strength decreases by a factor of more than 10 at coordinate $x = W_p$ (Figures 2 and 5, *a*), and a source with an „unlimited“ concentration of carriers (holes) is formed. This indicates that the process proceeds further with a significant contribution from the SCLC mechanism. A similar process also develops at the n^+-contact, the only difference being that the drift velocity of a hole packet is lower. This is attributable to their lower mobility, and a sharp reduction in the hole concentration to a negligible value occurs within ~ 100 ps, whereas ratio $n \ll N_{pl}$ for electrons near the p^+-contact is achieved at $t \approx 20$–30 ps.

A comparison of the figures presented above reveals that the shape of distributions $E(x)$, $n(x)$, and $p(x)$ is perfectly consistent with the model of a long-range ion track. The carrier drift kinetics gives rise to compression of an $e-h$ pair packet from both sides. Similar temporal variations of distributions also occur at higher concentrations of $e-h$ pairs, but the characteristic time values depend on N_{pl}.

The dependences of key characteristics of the kinetics of carrier outflow from a long-range ion track obtained by simulation and analytical calculation are compared below. The dependences of E_{pl}, $E_{\max\_p}$, and polarization layer thickness W_p near the p^+-contact on time ($t \leq 4$ ns) and the current signals for different N_{pl} are presented in Figures 5 and 6. Solid and dashed curves represent the results obtained by simulation and analytical calculation, respectively.

The results of modeling indicate that all changes related to track polarization occur within tens or hundreds of picoseconds. Specifically, E_{pl} decreases quickly from $E_{pl}(0) \approx 6.7$ kV/cm to 2 and 1 kV/cm at $t = 400$ and 800 ps, respectively, and the rate of its reduction increases with increasing N_{pl} (Figure 5, *a*). Dependence $E_{\max\_p}(t)$ is non-monotonic (Figure 5, *b*). At $N_{pl} = 1 \cdot 10^{15}\,\mathrm{cm}^{-3}$, a peak forms within ~ 400 ps. The strength in it reaches $1.4 \cdot 10^5$ V/cm, which is more than an order of magnitude higher than the average field in the detector at $t = 0$. The overall dependence of peak $E_{\max\_p}$ on N_{pl} is sublinear; at $N_{pl} = 1 \cdot 10^{17}\,\mathrm{cm}^{-3}$, its height is $1.3 \cdot 10^6$ V/cm.

It should be noted that a field strength of $\sim 10^5$ V/cm is already within the range of values initiating impact ionization of carriers, and $E_{\max\_p} = 1.3 \cdot 10^6$ V/cm should give rise to an avalanche breakdown of the p^+-n junction. The lack of such a breakdown in experiments with heavy

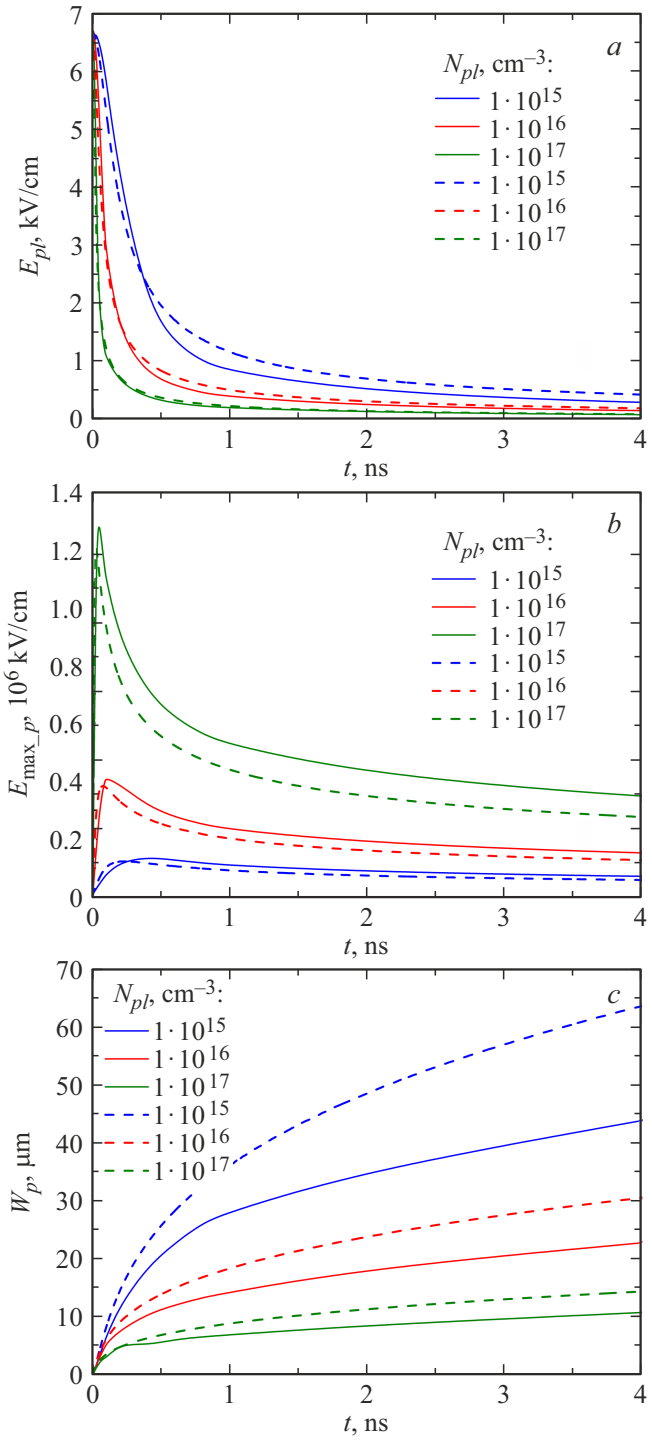

Figure 5. Temporal dependences of the electric field strength in track plasma (a), the maximum strength near the p^+-contact (b), and polarization layer thickness W_p (c) at different N_{pl}. Solid and dashed curves represent the results of simulation and analytical calculation, respectively.

ions may be attributed to a rapid reduction of the field strength with time. The $W_p(t)$ dependence is sublinear (Figure 5, c); at a fixed t, the smallest W_p value corresponds to the maximum concentration of $e-h$ pairs in track plasma, which is a factor contributing to the emergence of a field peak with a critically high strength.

A comparison of the results of analytical calculation of E_{pl}, E_{max_p}, and W_p with the corresponding simulated data (Figure 5) reveals a fine qualitative and quantitative agreement between the kinetics of variation of these parameters. The $W_p(t)$ curves are exceptions: calculated thickness W_p for them is greater than the values obtained by modeling; the most significant discrepancy is observed at $N_{pl} = 1\cdot10^{15}$ cm^{-3}.

In addition, the time needed to reach the E_{max_p} peak, which is the time of formation of the polarization layer, determined in modeling (Figure 5, b)) is longer than the corresponding calculated value. The values of t corresponding to this peak at $N_{pl} = 1\cdot10^{15}$, $1\cdot10^{16}$, and $1\cdot10^{17}$ cm^{-3} are 400, 150, and 45 ps in modeling and 225, 80, and 20 ps in calculations, respectively. These discrepancies are attributable to the fact that the non-uniform distribution of concentration of drifting carriers in the polarization region and the formation of a polarization layer near the n^+-contact were neglected in analytical calculations. The condition of saturation of the drift velocity of holes in the polarization region and the maximum and constant values of electron mobility in plasma were also introduced in calculations. Thus, the sublinear growth of drift velocity with the electric field strength to its saturation was neglected, while the simulation did not rely on the above simplifying assumptions.

The simulation and calculation of current pulse $J(t)$ revealed that its amplitude is proportional to N_{pl} and assumes a value of $1.5\cdot10^3$ A/cm^2 at $N_{pl} = 1\cdot10^{15}$ cm^{-3}. Figure 6 shows normalized current density pulses J_{norm} for different N_{pl} within the time interval of 0–2 ns. The pulse rise time is 1–2 ps regardless of N_{pl}. At larger t, the current kinetics is qualitatively similar to the variation of electric field strength in the plasma track region, which is a consequence of the formation of polarization layers near the contacts that is

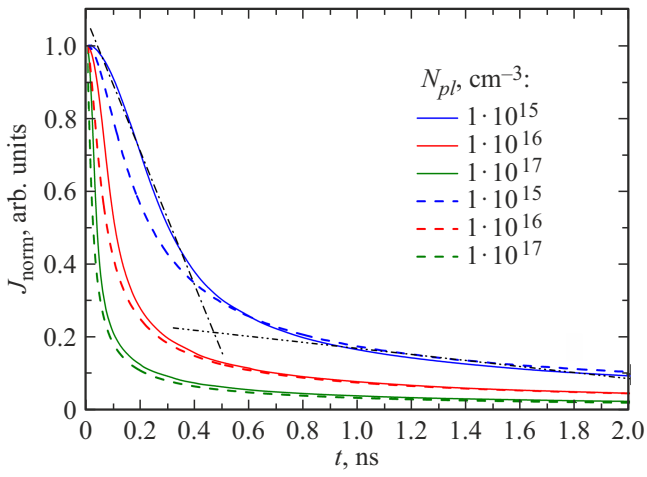

Figure 6. Normalized current density pulses for various N_{pl}. Dash-and-dot lines represent linear approximations of the signal within the time intervals of its fast and slow decay at $N_{pl} = 1\cdot10^{15}$ cm^{-3}.

coordinate with the evolution of $E(x)$ upon a reduction in the concentration of drifting holes near the p^+-contact with time and a reduction in the rate of hole outflow from the track at $x = W_p$ due to an enhancement of the role of the SCLC mechanism. The decay time of current corresponding to the track polarization stage was determined as the intersection point of linear approximations in the regions of its fast and slow decay (dash-and-dot lines in Figure 6). This time decreases in proportion to $\lg N_{pl}$, assuming the values of 480, 200, and 100 ps at N_{pl} equal to $1 \cdot 10^{15}$, $1 \cdot 10^{16}$, and $1 \cdot 10^{17}$ cm^{-3}, respectively. The last signal stage is a slow relaxation process caused by the depletion of electron-hole plasma in the central region of the track, where E_{pl} decreases with a reduction of the plasma layer thickness.

4. Conclusion

A quantitative model of signal formation in a silicon p^+-n-n^+-detector interacting with a long-range heavy ion was proposed, and an analytical description of the process was obtained. Novel calculated and simulated data revealed the following.

1. The current signal of a detector has two components: a fast polarization component, which is related to the formation of layers with a high electric field strength near the p^+- and n^+-contacts, and a slow relaxation component associated with vanishing of a plasma track.

2. Both components are governed by the drift transport of carrier packets that form track plasma, which results in the release of electrons and holes from it.

3. The current peak in the polarization signal component is a fundamental feature of current outflow from plasma of a long-range heavy ion.

4. The rise time of the current signal in the polarization component is not limited by the processes of current outflow from track plasma and is specified by the track creation time (several picoseconds), which is the time of flight of an ion through the sensitive region of a detector.

5. The decay time of the current signal is 480, 200, and 100 ps for N_{pl} equal to $1 \cdot 10^{15}$, $1 \cdot 10^{16}$, and $1 \cdot 10^{17}$ cm^{-3}, respectively.

The obtained results provide an adequate description of the polarization component of current, while the relaxation component requires 3D modeling of drift processes in the radial direction, which is beyond the scope of the present study. The proposed model of current outflow from a long-range ion track may be used to plan experiments with heavy ions and design high-speed electronics needed for signal detection.

Conflict of interest

The authors declare that they have no conflict of interest.

References

[1] P.A. Tove, W. Seibt. Nucl. Instrum. Meth. A, **51**, 261 (1967).
[2] W. Seibt, K.E. Sundström, P.A. Tove. Nucl. Instrum. Meth. A, **113**, 317 (1973).
[3] E.C. Finch. Nucl. Instrum. Meth. A, **113**, 41 (1973).
[4] S. Aiello, A. Anzalone, M.G. Campisi, G. Cardella, Sl. Cavallaro, E. De Filippo, E. Geraci, M. Geraci, P. Guazzoni, M.C. Iacono Manno, G. Lanzalone, G. Lanzano, S. Lo Nigro, A. Pagano, M. Papa, S. Pirrone, G. Politi, F. Porto, F. Rizzo, S. Sambataro, M.L. Sperduto, C. Sutera, L. Zetta. Nucl. Instrum. Meth. A, **427**, 510 (1999).
[5] Scientific program of the Super-FRS collaboration: report of the collaboration to the FAIR management, GSI Report 2014-4. https://repository.gsi.de/record/67533. DOI: 10.15120/GR-2014-4
[6] V. Eremin, O. Kiselev, N. Egorov, I. Eremin, Yu. Tuboltsev, E. Verbitskaya, A. Gorbatyuk. Nucl. Instrum. Meth. A, **796**, 158 (2015). http://dx.doi.org/10.1016/j.nima.2015.05.022
[7] V. Eremin, A. Bezbakh, I. Eremin, N. Egorov, A. Fomichev, M. Golovkov, A. Gorshkov, A. Galkin, O. Kiselev, A. Knyazev, D. Kostyleva, S. Krupko, D. Mitina, R. Slepnev, P. Sharov, E. Verbitskaya. JINST **12**, C03001 (2017). DOI: 10.1088/1748-0221/12/03/C03001
[8] D. Kostyleva, O. Kiselev, A. Bezbakh, V. Chudoba, V. Eremin, A. Fomichev, A. Gorshkov, S. Krupko, I. Mukha, I. Muzalevskii, C. Scheidenberger, P. Sharov. Acta Phys. Polonica B, **49** (3), 503 (2018). DOI: 10.5506/APhysPolB.49.503
[9] O.A. Kiselev, I. Mukha, C. Nociforo, A. Prochazka, F. Schirru, H. Simon, I. Eremin, V. Eremin, N. Fadeeva, E. Terukov, Yu. Tuboltsev, E. Verbitskaya, A.A. Bezbakh, A.S. Fomichev, M.S. Golovkov, A.V. Gorshkov, A.G. Knyazev, D.A. Kostyleva, S.A. Krupko, R.S. Slepnev, N. Egorov, S. Golubkov. Proc. Int. Symp. on Exotic Nuclei (EXON2014), p. 607 (2015). ISBN 978-981-4699-45-7
[10] J. Vesić, S. Saha, M. Górska, P. Boutachkov, G. Benzoni, J. Gerl, H. Weick, J. Winfield, S. Pietri, C. Nociforo, N. Pietralla, G. Guastalla, M. Winkler, H. Geissel. Nucl. Instrum. Meth. A, **1047**, 167714 (2023). DOI: 10.1016/j.nima.2022.167714
[11] T. Dickel, Ch. Hornung, D. Amanbayev, S.A. San Andrés, S. Beck, J. Bergmann, H. Geissel, J. Gerl, M. Górska, L. Gröf, E. Haettner, J.-P. Hucka, D.A. Kostyleva, G. Kripko-Koncz, A. Mollaebrahimi, I. Mukha, S. Pietri, W.R. Plaß, Z. Podolyák, S. Purushothaman, Jianwei Zhao. Nucl. Instrum. Meth. B, **541**, 275 (2023). DOI: 10.1016/j.nimb.2023.05.018
[12] L.V. Grigorenko, B.Yu. Sharkov, A.S. Fomichev, A.L. Barabanov, V. Bart, A.A. Bezbakh, S.L. Bogomolov, M.S. Golovkov, A.V. Gorshkov, S.N. Dmitriev, V.K. Eremin, S.N. Ershov, M.V. Zhukov, I.V. Kalagin, A.V. Karpov, T. Katayama, O.A. Kiselev, A.A. Korsheninnikov, S.A. Krupko, T.V. Kulevoi, Yu.A. Litvinov, E.V. Lychagin, I.P. Maksimkin, I.N. Meshkov, I.G. Mukha, E.Yu. Nikol'skii, Yu.L. Parfenova, V.V. Parkhomchuk, S.M. Polozov, M. Pfutzner, S.I. Sidorchuk, H. Simon, R.S. Slepnev, G.M. Ter-Akop'yan, G.V. Trubnikov, V. Chudoba, K. Scheidenberger, P.G. Sharov, P.Yu. Shatunov, Yu.M. Shatunov, V.N. Shvetsov, N.B. Shulgina, A.A. Yukhimchuk, S. Jaramyshev. Phys. Usp., **62**, 675 (2019). DOI: https://doi.org/10.3367/UFNr.2018.07.03838

[13] C. Cazzaniga, M. Kastriotou, R.G. Alía, P. Fernandez-Martinez, V. Wyrwoll, T. Minniti, Ch.D. Frost. Nucl. Instrum. Methods A, **985**, 164671 (2021). https://doi.org/10.1016/j.nima.2020.164671
[14] G. Filatov, A. Slivin, A. Agapov et al. In Proc. 13th Int. Particle Acc. Conf. IPAC2022 (Bangkok, Thailand, 12–17 June 2022), JACoW Publishing, p. 3096. DOI: 10.18429/JACoW-IPAC2022-THPOMS054
[15] N.N. Fadeeva, V. Eremin, E. Verbitskaya, I. Eremin, Yu. Vidimina. St. Petersburg Polytech. University. J. Phys. and Math., **16** (1.2), 295 (2023). https://doi.org/10.18721/JPM.161.245
[16] S.M. Sze, K.K. Ng. *Physics of semiconductor devices.* 3rd edn (J. Wiley & Sons, Inc., Hoboken, N. J., 2007).

Translated by D.Safin